Large Eddy Simulation of Transition of Free Convection Flow over an Inclined Upward Facing Heated Plate

Ali S. Alzwayi[a], Manosh C. Paul[a1] and **Salvador Navarro-Martinez[b]**

[a]Systems, Power & Energy Research Division, School of Engineering, University of Glasgow, Glasgow G12 8QQ, UK

[b]Department of Mechanical Engineering, Imperial College London, London SW7 2AZ, UK

Abstract

Transition of free convection flow of air over an inclined heated surface is investigated numerically by using a Large Eddy Simulation method. In particular, we focus on how inclination angle of an upward-facing heated plate affects flow transition. Special attention is paid to the development of the thermal boundary layer and the transition from the laminar to turbulent stage. Results show that the transition occurs early when the plate is moved from its vertical position due to the rapid growth of both the velocity and thermal boundary layers. As a consequence, the critical Grashof number drops. Effects of the inclination of plate on the turbulent velocity fluctuations are also investigated, and the predicted results are in very good agreement with various experimental data available in the literature.

Key words: Boundary layer, Free convection, Transition, Turbulence, Large Eddy Simulation

[1] Corresponding author: Manosh.Paul@glasgow.ac.uk, Tel: +44(0) 141 330 8466

List of Symbols

Roman Symbols

Cs	Smagorinsky model constant
g	Gravitational acceleration
Gr	Grashof number
L	length of the plate
n_x, n_y, n_z	number of nodes in the x, y and z directions respectively
Nu	Nusselt number
P	pressure
Pr	Prandtl number
S_{ij}	strain rate tensor
T	temperature
t	time
u_i or u, v,w	velocity components in the Cartesian coordinates
x_i or x, y, z	Cartesian coordinate directions

Greek Symbols

¸	angle of inclination with respect to the vertical position
²	thermal expansion coefficient
•	diffusion coefficient for energy transport
”	filter width
μ	molecular viscosity of fluid
$Á$	fluid density
$Ä_{ij}$	subgrid scale stresses

Subscripts

a	air
c	critical
•	ambient conditions
sgs	sub-grid scale
max	maximum
P	plate
rms	root mean squares

1. Introduction

Transition of a thermal boundary layer over an inclined heated plate has received significant attention over the years due to its wide range of applications in engineering systems: such as transistors, mainframe computers, heat exchangers, solar energy collectors, and nuclear reactor cooling elements. Rich [1] carried out experiments of laminar free convection flow on a heated plate with its angular orientation varying from 0° to 45°, while later Kierkus [2] focused on two-dimensional analysis of laminar free convection and satisfactorily compared his results with the experimental data of Rich [1].

Hassan and Mohamed [3] measured the local heat transfer on an isothermal plate. The angle of inclination was varied from -90° to 90°, as the study particularly focused on the transition of flow on both the downward and upward facing heated surfaces. However, their results did not show any transition stage on the downward facing heated surface due to the relatively short length of the plate used in the experiment. For the same reason, they could not predict the transition stage in the vertical case. Nevertheless, the transition behaviour for the upward plate case was summarised, and correlation equations for important flow parameters were suggested at the transition region.

Tritton [4], on the other hand, used a fibre anemometer method to capture transition as well as the development of full turbulence on an isothermal plate. The experiment was performed in air and the Grashof number (ratio bouyancy to viscous forces) on a vertical plate was recorded to be 9.26×10^6, which is much smaller than Grashof numbers found in other experiments. Tritton suggested that this behaviour was mainly due to the strong flow disturbances in his experimental set-up and possible uncertainties in the methods he used. Sparrow and Hussar [5] and Lloyd and Sparrow [6] established later a correlation between the inclination angle of a heated plate and the instability of the thermal boundary layer. Their results showed that the onset of transition was characterised by longitudinal vortices. Similarly, Gebhart [7] studied two different types of instability, thermal and hydrodynamic, in buoyancy induced flows. Their effects on the flow transition were investigated on a vertical, a horizontal and an inclined surface, respectively.

Later, Black and Norris [8] provided a method for flow visualisation and measured local heat transfer coefficient for the natural convection on an inclined isothermal plate. They particularly found that the thermal sub-layer contains thermal waves that traverse the heated

plate and cause significant variations in the local heat transfer. Recently, natural convection over an upward facing inclined plate was examined by Komori e*t al.* [9] and Kimura et *al*. [10], where the plates were kept under the heat flux thermal conditions in order to study the mechanism of transition from laminar to turbulent flow. The flow over the heated plate and the wall temperature were visualised by fluorescent paint and a liquid–crystal thermometry respectively. Komori *et al.* [9], showed that the separation of the boundary layer and the onset of streaks appear when the modified Rayleigh number exceeds a characteristic value. Nevertheless, the complete transition process was not fully examined.

Recently, Paul et *al*. [11] studied the effects of plate angle on the thermal boundary layer stability. They investigated the influence of high order effects of the boundary layer on the vortex instability of thermal boundary layer flow in a wedge-shaped domain formed by the heated and the outer boundary surface. Most recently, Alzwayi and Paul [12] numerically investigated the transition of a thermal boundary layer in a vertical parallel plate channel and its dependence on plate width and temperature. In the context of a heated surface facing downward, Alzwayi and Paul [13] also studied the transition of free convection flow in an inclined parallel walled channel. They investigated the effects of inclination angle and width of the channel on transition. However, very little is known about the transition of flow developing on a heated surface facing upward and how it is affected by its inclination angle.

The aim of this paper is therefore to carry out an investigation on the transition phenomena of a free convection flow developing on an inclined heated plate by Large Eddy Simulation (LES). The paper focus on how the flow and thermal fields jointly affect the transition process and the effects they have on the turbulent quantities such as fluctuating velocity components, which are generated after the flow transition.

2. Model geometry

A schematic drawing of the model geometry and computational domain with coordinate systems is given in Fig. 1. An isothermal heated plate, temperature of which is denoted by *Tp*, is exposed to the environment at an ambient temperature denoted by *Ta.* Driven by the buoyancy force, the air heated up by the hot wall flows along the heated surface and forms natural convection boundary and thermal layers. The length of the plate in the *y* direction ($L=L_y$) is 3 m. The free boundary opposite to the plate is placed at a distance equal to 3.5

times the thickness of the fully developed boundary layer at the downstream (which corresponds to $L_x \approx 1$m. A periodic boundary condition is implemented in the spanwise direction in the *z*-direction, with the boundaries separated 1.5 m.

3. Mathematical model

3.1 Governing equations

Free convection over the heated plate is governed by the three-dimensional unsteady-state Navier–Stokes equations together with the energy equation. The working fluid (air with *Pr*=0.71) flow is considered to be Newtonian and all the physical properties of air are assumed to be constant. The filtered governing equations of flow and energy for large eddy simulations, which are subject to the Boussinesq approximation, take the following forms:

$$\frac{\partial \rho}{\partial t} + \frac{\partial \rho \overline{u}_i}{\partial x_i} = 0 \tag{1}$$

$$\frac{\partial \rho \overline{u}_i}{\partial t} + \frac{\partial \rho \overline{u}_j \overline{u}_i}{\partial x_j} = -\frac{\partial \overline{P}}{\partial x_i} + \frac{\partial}{\partial x_j}\left(\mu \frac{\partial \overline{u}_i}{\partial x_j}\right) - \frac{\partial \tau_{ij}}{\partial x_j} + \rho \overline{g}_i \tag{2}$$

$$\frac{\partial \rho \overline{T}}{\partial t} + \frac{\partial \rho \overline{u}_j \overline{T}}{\partial x_j} = \frac{\partial}{\partial x_j}\left(\Gamma \frac{\partial \overline{T}}{\partial x_j}\right) - \frac{\partial J_j^{sgs}}{\partial x_j} \tag{3}$$

where $\overline{g}_i = \left[g \sin\theta\beta\left(\overline{T} - \overline{T}_\infty\right), g\cos\theta\beta\left(\overline{T} - \overline{T}_\infty\right), 0 \right]$, $\Gamma = \mu/Pr$ is the diffusion coefficient, x_j is the coordinate system and u_j is the corresponding velocity components. *P* is the pressure, *Á* is the density, μ is the dynamic viscosity, and *Pr* is the Prandtl number of air. The spatial filter applied to obtain the governing LES equations separates the large scale (resolved scale) flow field from its small scale (sub-grid scale), Leonard [14]. The effects of the small scales, appear in the sub-grid stress terms, defined as

$$\tau_{ij} = \rho\overline{u_i u_j} - \rho\overline{u}_i\overline{u}_j \tag{4}$$

and

$$J_j^{sgs} = \rho\overline{u_j T} - \rho\overline{u}_j\overline{T} \tag{5}$$

which are unknown and referred to the sub-grid scale stresses and the sub-grid scale scalar fluxes respectively. The Smagorinsky model [15], is used to represent the sub-grid scale stresses, viz

$$\tau_{ij} - \frac{1}{3}\tau_{kk} = \rho\left(Cs\Delta\right)^2 \left\|\overline{S}_{ij}\right\| \overline{S}_{ij} \tag{6}$$

The sub-grid dynamic eddy viscosity is obtained from $\mu_{sgs} = \rho\left(C_S\Delta\right)^2 \left\|\overline{S}_{ij}\right\|$ and the unknown Smagorinsky constant, C_s is calculated by using the "localized" dynamic model of Piomelli and Liu [16]. The magnitude $\left\|\overline{S}_{ij}\right\| = \sqrt{2\overline{S}_{ij}\overline{S}_{ij}}$ is the Frobenius norm of the resolved scale strain rate tensor $\overline{S}_{ij} = \frac{1}{2}\left(\frac{\partial \overline{u}_i}{\partial x_j} + \frac{\partial \overline{u}_j}{\partial x_i}\right)$. For the sub-grid scale scalar fluxes, a gradient model proposed by Schmidt and Schumann [17], is applied:

$$J_j^{sgs} = -\rho\Gamma_{sgs}\frac{\partial \overline{T}}{\partial x_j} = -\rho\frac{\mu_{sgs}}{\sigma_{sgs}}\frac{\partial \overline{T}}{\partial x_j} \qquad (7)$$

where $\tilde{A}_{sgs}$ is the sub-grid scale Prandtl/Schmidt number which is here assigned a value of 0.71.

3.2 Boundary conditions

The following boundary conditions are used for the LES equations (1-3): At the inlet the velocity and temperature boundary conditions are applied, viz:

$$\overline{u} = 0\,, \qquad \frac{\partial \overline{v}}{\partial y} = 0\,, \qquad \overline{w} = 0\,, \qquad \text{and} \qquad \overline{T} = \overline{T}_\infty\,,$$

While, at the outlet boundary, a zero gradient condition of the form $\frac{\partial \overline{u}_i}{\partial n} = 0$ where $\frac{\partial}{\partial n}$ denotes the gradient taken to the normal outflow boundary, has been used which was sufficient to minimise any effects of the outlet boundary in the solution. At the heated plate, no-slip condition is applied at a constant temperature denoted by T_P. A free boundary condition is employed at the side opposite to the heated plate; while in the spanwise direction, a periodic boundary condition is employed.

4. Overview of the numerical methods

An in-house FORTRAN code, LES-BOFFIN (Boundary Fitted Flow Integrator), which was initially developed at the Imperial College London for simulating turbulent reacting flow, has been modified and extended to solve the governing equations for free convection flow. The code is fully implicit and second order accurate in both space and time. The BOFFIN code has been applied to simulate turbulent flow in other engineering contexts, see for examples Dodoulas et al [18], Jones *et al*. [19] Paul *et al*. [20], Jones and Paul [21], Paul and Molla [22] and references therein.

The governing filtered equations (1-3) are solved in using the finite volume approach. The velocities are stored in a staggered arrangement while the scalars are stored in the centre of the cell. Central differences have been used to discretize the momentum equations. In order to preserve the bounds of the scalar field and avoid spurious oscillations; a Total Variation Diminishing (TVD) scheme, e.g. see Sweby [23], has also been used for the convective terms in the energy equation. A conjugate-gradient solver (Kershaw [24]) is used for the Pressure correction. The flow solver is then marched in time using a Crank-Nicholson scheme and is formally second order in space and time (away from discontinuities). More details about the numerical algorithm are given in the cited references above as well as in the reference papers therein.

5. Grid resolution study

The numerical results to be presented are tested first for their dependence on a set of grid resolutions as shown in Fig. 2. Four grids are used to study one case and the results of air velocity and temperature in the laminar and turbulent stages are compared with the experimental data of Tsuji and Nagano [25] and Yan and Nilsson [26]. This mesh dependence test was performed by changing the total number of grid nodes in the three directions *y*, *x* and *z* as (n_y), (n_x), (n_z) respectively, which are 256 × 96 × 96, 292 × 124 × 96, 320 × 144 × 96 and 340 × 164 × 96. The grid is non-uniform and refined in the region upstream as well as close to the wall, where large gradient of velocity and temperature are present. The grid refinement is done by using a stretching cell ratio of 1.016 in both the *y* and *x* directions, while in the *z* direction the mesh distribution remains uniform.

As we can see in Fig. 2 (a) and (b) that the first grid 256 × 96 × 96 provides an overestimation in the velocity and temperature of the flow within the laminar region. However, the next three grids, 292 × 124 × 96, 320 × 144 × 96 and 340 × 164 × 96, produce satisfactory results, and the relative difference found in the finer meshes is very small. All these grids are in excellent agreement with the experimental data of Tsuji and Nagano [25]. Therefore, either of these three grids could be used, however to avoid any undesirable discrepancies in the numerical results the grid size of 320 × 144 × 96 is chosen to perform all the numerical simulations with a fixed timestep dt of 10^{-3} secs.

The LES code is fully parallel with an Open-MPI interface to communicate and share data among the multiple central processing units (CPUs) of a HPC cluster “miffy” available at the University of Glasgow. A total of 16 CPUs were used and each simulation took a wall-clock time of about 3 days to complete and reach to a statistically stationary result.

6. Results and discussions

6.1 Transition toward turbulence

In this section we reported the sequence of events that lead to the onset of turbulence. First, unsteady flow development and structures on a vertical plate are presented in Fig. 3 in a mid-location, in terms of the velocity and temperature fields, at three different time instances, e.g. 5s, 8s and 12s. The contour plots are zoomed in the upstream location, 0 d *y* d 1.3 m, to better visualise the occurrence of the flow separation evolving upstream within the vertical location. Previous studies suggested that the laminar boundary layer developing over the uniformly heated surface becomes unstable to a specific distance downstream. The contour plots in Figs. 3 (a) and (e) shows the initial breakdown of the laminar boundary layer, which amplifies and then produces three-dimensional shear layers with concentrated turbulent bursts. These bursts are known to “consume” the laminar boundary layer region within the transition region; however, with an increase in time to 8 and 12 seconds the initial plume starts to expand and rise, causing an increase in the thickness of the boundary layer in the turbulent region as clearly shown in Fig. 3 (b), (c) and (d).

The structure of the thermal boundary layer in the three-dimensional filed is presented in Fig. 3 (h). The fluid temperature varies along the plate with a very green dark colour showing a low temperature especially in the bottom of the plate near the inlet section, while in the downstream the green colour appears as the temperature becomes relatively large there. The surface temperature can be used to determine the local heat transfer coefficients as done in Alzwayi and Paul [12, 13]. This local heat transfer coefficient will be large in the low temperature region towards the downstream regime but small in the high temperature located in the upstream where the streaks and waves started to develop along the flow. Lloyd and Sparrow [6] stated that the onset location of these streaks is same as the position at which the flow takes the transition from its laminar to turbulent stage.

Similar sets of visualisation are carried out in Fig. 4 with an inclination plate of ¸ = 45°, where the breakdown in the laminar boundary layer initially starts (a, e) with a gradual increase in the thickness of the boundary layers compared to that seen in the vertical case. As the simulation time progresses, Fig. 4 (b) and (c) show that the thickness of the flow as well as the thermal boundary layers becomes larger and widely spreads after a large expansion of the plume. As a result, the separation point of the flow shifts some distance towards the downstream with more unstable flow developed at the outer edge of the boundary layer.

6.2 Visualisation of three-dimensional boundary and thermal layers

Iso-surface contour plots of the flow field and temperature in the whole computational domain are shown in Figs. 5 and 6 respectively at four different chosen angles, 0°, 20°, 45° and 70°. In general for the vertical plate at ¸ = 0° the thickness of the boundary and its thermal layers reach their maximum at the outlet section as shown in Fig. 5 (a). With an increase in the plate angle to 20° their maximum value is still located at the outlet section, however the surface of the top shape becomes more flat compared to that in the vertical case especially in the boundary layer field where its top-surface is very sharp.

Fig. 5 (c) at ¸ = 45° shows that the maximum value of the thickness at the outlet section disappears and the growth of both the boundary layers is likely to become flat along the plate. The same behaviour of the development of the thermal boundary layer can been in Fig. 6. However, with an increase in the plate inclination to 70°, the growth of both the boundary and thermal layers is widely disturbed, and the location of their maximum moves backward near the middle of the plate. This behaviour of the boundary layer development can be explained by the fact that in the vertical plate the only component of the buoyance force acts in the flow direction, which increases as the length of the plate is increased. Whereas, in the case of an inclination heated plate facing upward, a second component of the buoyance force exists in the direction away from the plate, which causes the pressure in the boundary layer to be lower than the surrounding. This pressure further influences the development of flow near the inlet; as a result both the boundary and thermal layer thicknesses are increased with a magnitude drop in the mean temperature and velocity.

6.3 Turbulent velocity fluctuations

Root mean squares (rms) of the turbulent velocity fluctuations occurring very near to the hated vertical surface are shown in Fig. 7 in the y and x directions as v_{rms}/v_{max} and u_{rms}/v_{max} respectively. These results are plotted as a function of the dimensionless transverse coordinate, $(x/y)\,Nu$, in order to make a direct comparison with various experimental data. The numerical profile of v_{rms}/v_{max} appears to have two peaks, the first one appears in the buoyant sub-layer region ($0.1 < (x/y)\,Nu < 1.0$) while the second one is in the outer region ($1.0 < (x/y)\,Nu < 10$), with a maximum situated at a position of the boundary layer beyond the location of the maximum velocity reported in Fig. 2 (d). This finding shows a good agreement with the experimental data of Smith [27]. The numerical results of v_{rms}/v_{max} have also an agreeable trend with the experimental data of Miyamoto and Okayama [28] at a Grashof number (Gr) of 4.84×10^{10}. On the other hand, the peak of u_{rms}/v_{max} appears in the outer region and agrees well with Kato et al. [29] who used a Laser Doppler anemometer to measure the air velocity. Tsuji and Nagano [25] at $Gr = 8.44 \times 10^{10}$ used a hot wire measurement technique for the velocity, which provides larger fluctuations in the buoyant sub-layer.

The distributions of the velocity *rms* along the heated plate are shown in Fig. 8 for ¸ = 0° and 70° and at different vertical locations of y, between 0.5 and 2.5 m. The component of the velocity fluctuation v_{rms} in the flow direction is likely to be zero at $y = 0.5$ m as the flow is in the laminar stage, shown in Fig. 8 (a). However, as the flow becomes fully developed downstream, the peak of the velocity fluctuation v_{rms} and u_{rms} increases gradually. At 70°, the two peaks of v_{rms} move away of the heated plate as also can be seen in Fig. 8 (d). Moreover, compared to the vertical case, the intensity of v_{rms} and u_{rms} also drops sharply for ¸ = 70° due to an increase in the boundary layer thickness, already explained in the contour plots in Fig. 5. However, the velocity fluctuation in the z-direction rises, as shown in Fig. 8 (f), with the peaks of w_{rms} recorded in the outer region of the boundary layer, e.g. when $x > 0.01$ m, and move to the buoyant sub-layer region for ¸ = 70°. This further indicates that the maximum velocity in the spanwise direction occurs very close to the heated plate.

Fig. 9 shows the contours plot of the velocity *rms* for four different angles 0°, 20°, 45° and 70°. In general, as the angle of the plate increases the magnitude of v_{rms} decreases in the y

direction, so the intensity of its fluctuation drops. The variation of v_{rms} shown for 70° in Fig. 9 (i) agrees with the field of velocity distribution presented in Fig. 5 (d). Overall, it can be seen that with an increase in the angle both the intensity of the velocity in the *y* and *x* directions drop but increases in the *w* direction.

6.4 Critical Grashof number

In the final figure, Fig. 10, the location of the transition taking place on the heated plate is summarised in terms of the critical Grashof number, which is determined by the critical distance from the local variation of the surface heat transfer coefficient (further details about the derivation are available in Alzwayi and Paul 2013). The value of $log(Gr_c\ Pr)$, corresponding to the point where the transition starts, compares generally well with experimental data of Al-Arabi and Sakr [30] and Hassan and Mohamed [3] obtained at the end of the transition stage (solid lines). While, there data recorded at the beginning of the transition stage (dashed lines) fall below the numerical results within the wider range of the plate orientation angles. The same behaviour is seen in the experimental data of Lloyd and Sparrow [6]. However, most of the experimental data for ¸ < 25° agrees reasonably well with the present numerical results. And in terms of understanding the transition behaviour of the flow, these results further confirm that an early transition occurs when the plate angle is increased.

7. Conclusion

Three dimensional large eddy simulations of free convection flow along an inclined heated plate have been carried out using an in-house developed LES-BOFFIN code. We reported that the predicted mean temperature and velocity in the turbulent and laminar flows over the vertical plate have good agreement with the experimental data. The *rms* of the velocity fluctuations also generally compared well.

Visualisations of the boundary layer and its thermal thickness are provided, which indicate that with an increase in the angle of the plate the boundary layers began to roll over the outer edge of the boundary layer after the transition. This leads to a fall in the mean velocity and temperature in the boundary layer.

The inclination of the plate increases the peak velocity fluctuation in the *y* direction as the v_{rms} moves out of the region of the boundary layer, while in the *z* direction the peaks of the velocity fluctuation w_{rms} move to the buoyant sub-layer region.

References

~~[2] J.R. Bodia, J.F. Osterle, The development of free convection between heated vertical plates. Journal of Heat Transfer, 84 (1962) 40-44.~~

[1] R. B. Rich, An investigation of heat transfer from an inclined flat plate in free convection, International Journal of Heat Mass Transfer, 11(1953) 241-253.

[2] W. T. Kierkus, An analysis of laminar free convection flow and heat transfer about an inclined isothermal plate, International Journal of Heat Mass Transfer, 11(1968) 241-253.

[3] k. Hassan, and , S. A. Mohamed, Natural convection from isothermal flat surfaces, International Journal of Heat Mass Transfer, 13 (1970) 1873-1886.

[4] D. J. Tritton, Transition to turbulence in the free convection boundary layers on an inclined heated plate, Journal of Fluid Mechanics, 16 (1963) 417-435.

[5] E. M. Sparrow, R. B. Hussar, Longitudinal vortices in natural convection flow on inclined plats, Journal of Fluid Mechanics, 39 (1969) 251-255.

[6] R. J. Lloyd, E. M. Sparrow, On the instability of natural convection flow on inclined plates, Journal of Fluid Mechanics, 42 (1970) 465-470.

[7] B. Gebhart, Instability, Transition, and Turbulence in Buoyancy-Induced flows, Annu. Rev. Fluid Mech, 5 (1973) 213-246.

[8] W. Z. Black, J. K. Norris [1975], The thermal structure of free convection turbulence from inclined isothermal surfaces and its influence heat transfer, International Journal of Heat Mass Transfer, 18 (1975) 43-50.

[9] F. Kimura, T. Yoshioka, K. Kitamura, M.Yamaguchi, and A.Toshihiko, Fluid flow and heat transfer of natural convection at slightly inclined upward facing heated plate, Heat Transfer – Asian Research, 31(2002) 362-375.

[10] K. Komori, S. Kito, T. Nakamura, Y. Inaguman, T. Inagaki, [2001], Fluid flow and Heat transfer in transition process of natural convection over an inclined plate, Heat Transfer – Asian Research, 30(2001) 648-689.

[11] M. C. Paul, D. A. S Rees M. Wilson, The influence of higher order effects on the vortex instability of thermal boundary layer flow in a wedge-shaped domain, International Journal of Heat and Mass Transfer, 48 (2005)1417–1424.
[12] A. S. Alzwayi and M. C. Paul, Effect of width and temperature of a vertical parallel plate channel on the transition of the developing thermal boundary layer, International Journal of Heat and Mass Transfer, 63 (2013)20-30.
[13] A. S. Alzwayi and M. C. Paul,Transition of free convection flow inside an inclined parallel walled channel: effects of inclination angle and width of the channel, International Journal of Heat and Mass Transfer, 68 (2014) 194-202.
[14] A. Leonard, Energy cascade in Large-Eddy Simulations of turbulent fluid flows, Adv Geophys, (1974) 237-248.
[15] J. Smagorinsky, General Circulation Experiments with the Primitive Equations-I. The Basic Experiment, Monthly Weather Review, 91(1963) 99-164.
[16] U. Piomelli, J. Liu, [1995], Large-eddy simulation of rotating channel flows using a localized dynamic model, Physics of Fluids, 7 (1995) 839-848.
[17] E. Schmidt, U. Schumann, [1989], Coherent Structure of the Convective Boundary Layer Derived from Large-Eddy Simulations, Journal of Fluid Mechanics, Vol. 200 (1989) 511- 562.
[18] I. A. Dodoulas, S. Navarro-Martinez Large Eddy Simulation of Premixed Turbulent Flame using the Probability Density Function Approach, Flow, Turbulence and Combustion, 90 (2013) 645-678.
[19] W. P. Jones, and S. Navarro-Martinez, Large Eddy Simulation of Auto-ignition with a sub-grid Probability Density Function method. Combustion and Flame, 150 (2007), 170-187.
[20] S. C, Paul, M. C. Paul W. P. Jones ,Large Eddy Simulation of a turbulent non-premixed propane-air reacting flame in a cylindrical combustor, Computers and Fluids, 39 (2010) 1832-1847.
[21] W. P. Jones, M. C Paul, Combination of DOM with LES in a gas turbine combustor, International Journal of Engineering Science, 43 (2005) 379-397.
[22] M.C. Paul, M. M. Molla, Investigation of physiological pulsatile flow in a model arterial stenosis using large-eddy and direct numerical simulations, Applied Mathematical Modelling, 36 (2012) 4393-4413.
[23] P. K. Sweby, [1984], High Resolution Schemes Using Flux Limiters for Hyperbolic

Conservation Laws, SIAM Journal on Numerical Analysis, 21 (1984) 995-1011.
[24] D. S. Kershaw, The Incomplete Cholesky-Cojugate Gradient method for the iterative solution of systems, J. Computational Physics, 26 (1978) 43-65.
[25] T. Tsuji, Y. Nagano, Turbulent measurements in a natural convection boundary layer along a vertical flat plate, International Journal of Heat Mass Transfer, 31 (1988) 2101-2111.
[26] Z. H. Yan, E. E. A . Nilsson, Large eddy simulation of natural convection along a vertical isothermal surface, Heat Mass Transfer, 41(2005), 1004-1013.
[27] R. R. Smith, Characteristics of Turbulence in Free Convection Flow Past a Vertical Plate", Ph.D. Thesis, (1972), Univ. of London.
[28] M. Miyamoto, M. Okayama, An experimental study of free turbulent free convection boundary layer in air along a vertical plate using LDV, JSME, Bulletin, 25 (1982) 1729-1736.
[29] S. Kato, S.Murakami, R. Yoshie, Experimental and numerical study on natural convection with strong density variation along a heated vertical plate, Ninth symposium on turbulent shear flows, Kyoto, Japan, August (1993) 1251-1256.
[30] M. AL-Arabi, and B. Sakr, [1988], Natural convection heat transfer from inclined isothermal plates, International Journal of Heat Mass Transfer, 31(1988) 559-566.

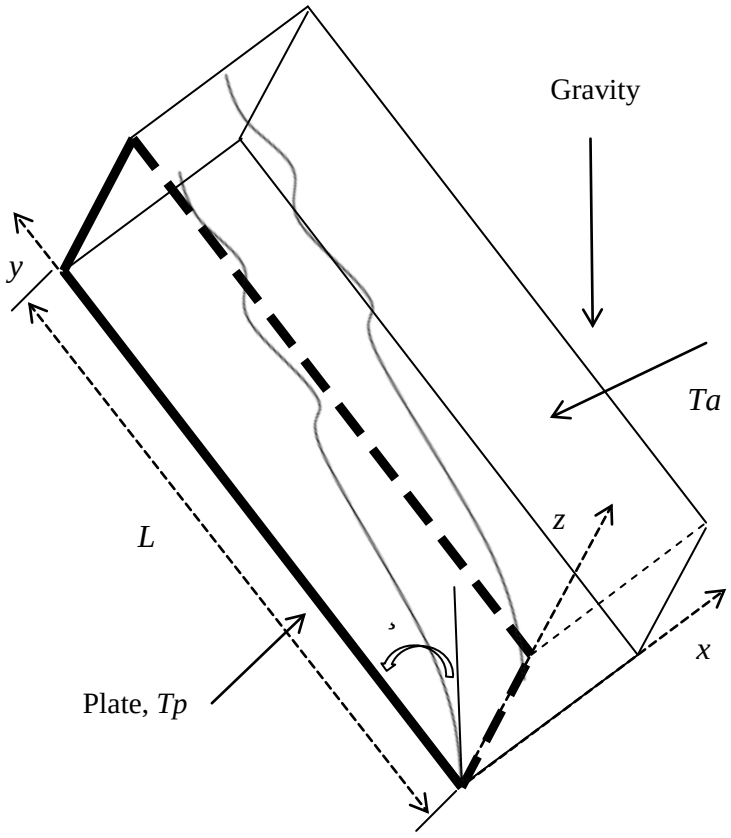

Fig. 1. Flow geometry with coordinate systems

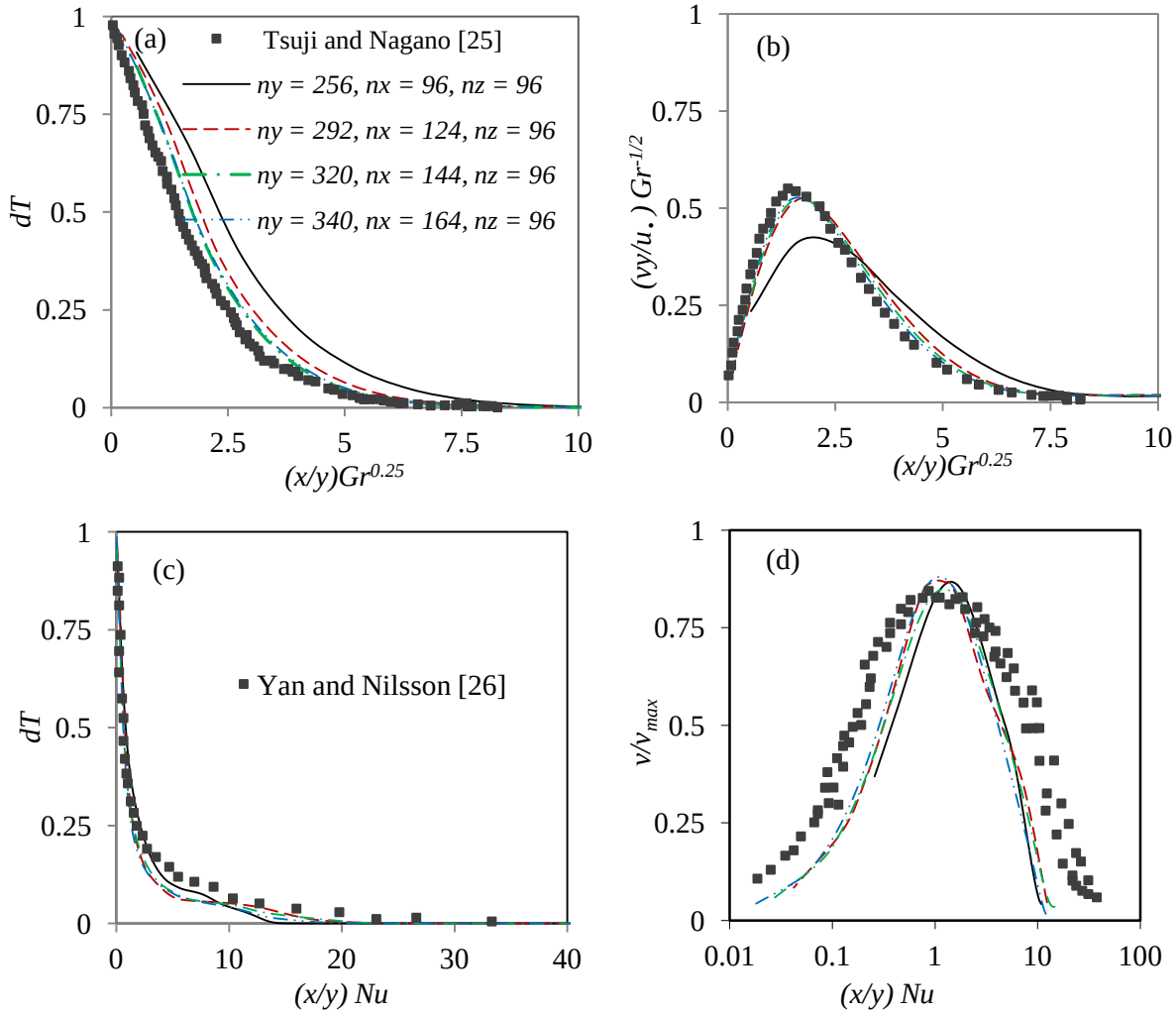

Fig. 2. Mesh dependence on the velocity and temperature results in the laminar stage (a, b) and turbulent stage (c, d).

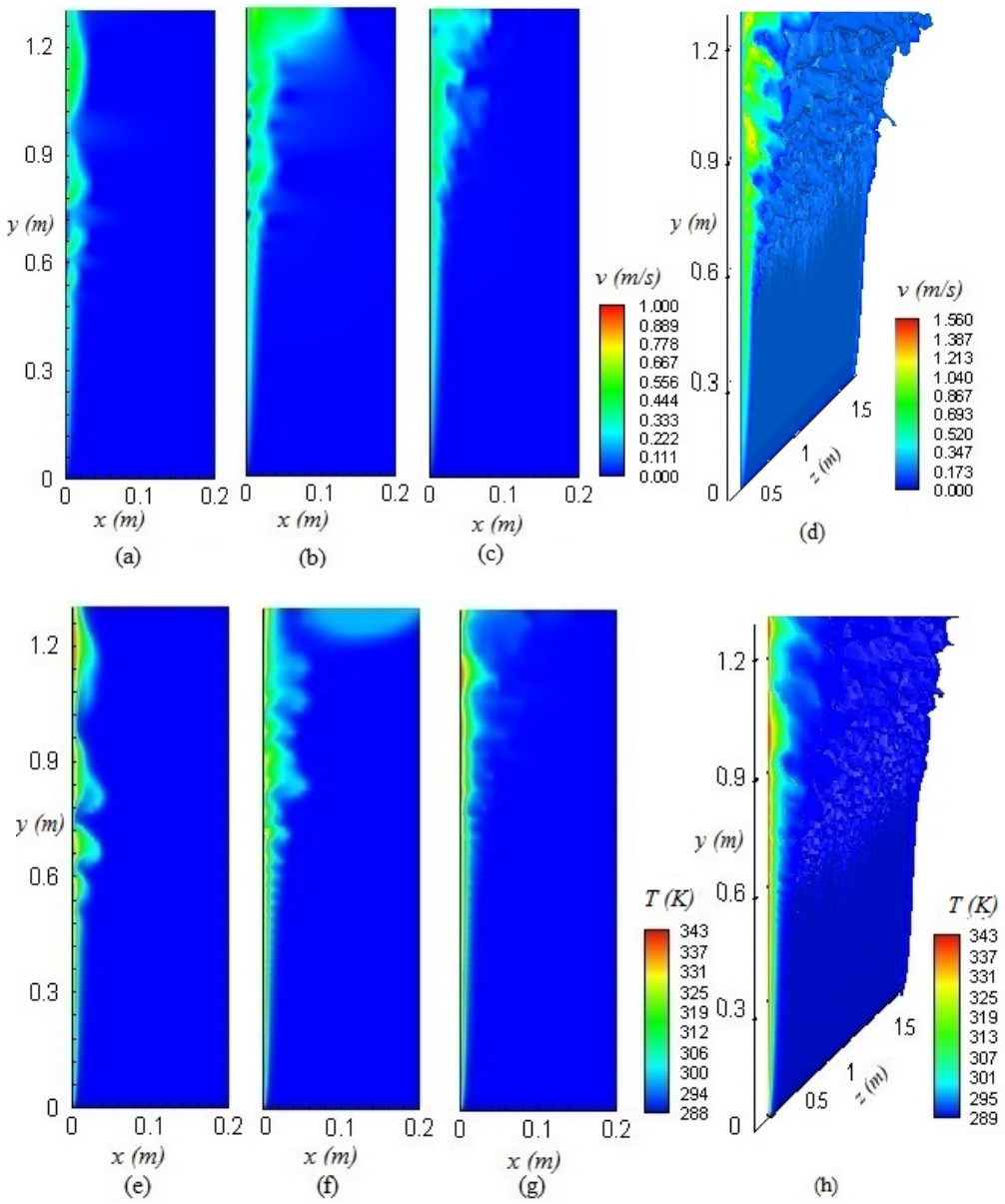

Fig. 3. Development of turbulent structure downstream on the vertical plate at ¸ = *0*°, where (a-c) the velocity contours and (e-g) the temperature contours at 5, 8 and 12 seconds respectively. A three–dimensional view of them at the final timestep is shown in frames (d) and (h) respectively.

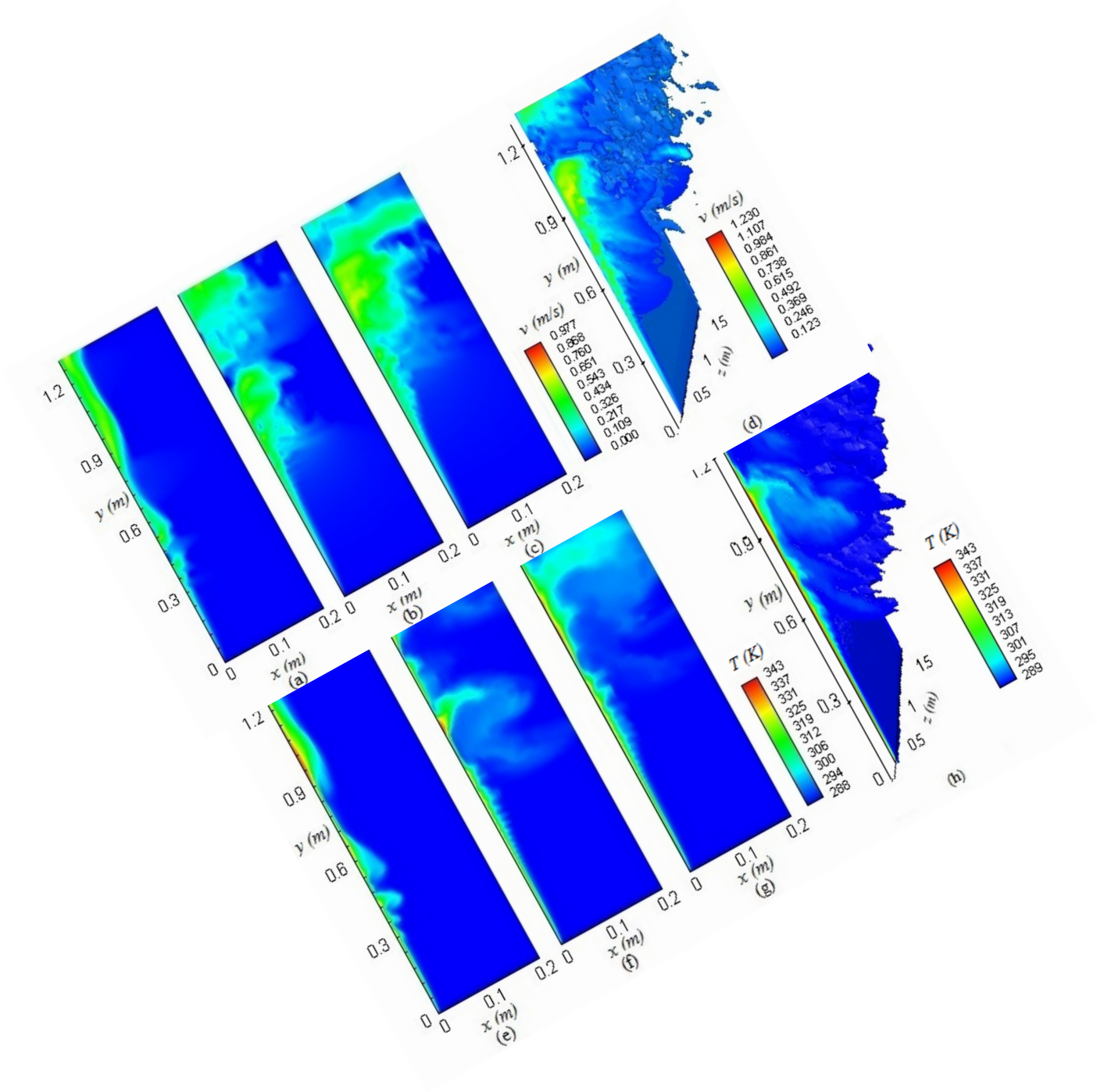

Fig. 4. Development of turbulent structure downstream at an inclination ¸ = *45*°, where (a-c) the velocity contours and (e-g) the temperature contours at 5, 8 and 12 seconds respectively. A three–dimensional view of them at the final timestep is shown in frames (d) and (h) respectively.

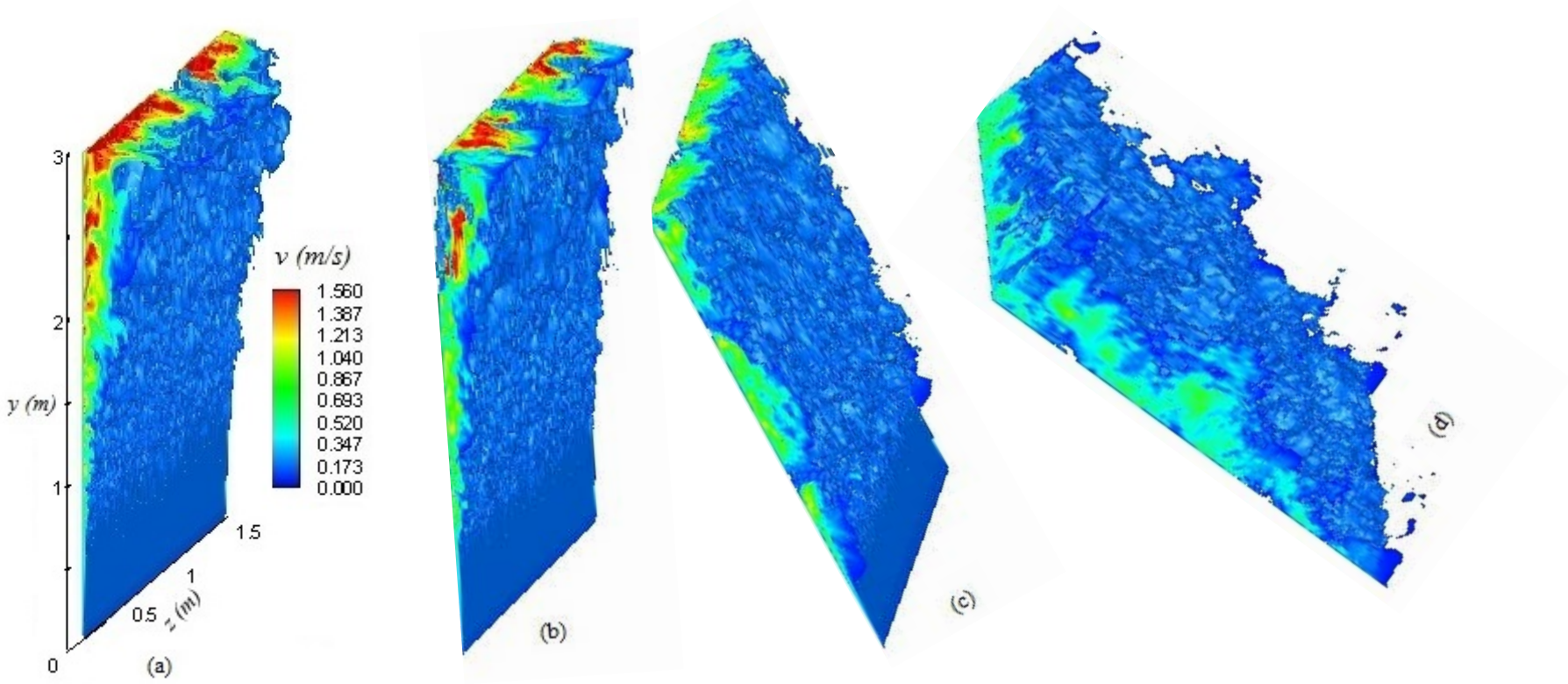

Fig. 5. Velocity iso-surface contour plots at ¸ = 0° (a), ¸ = 20° (b), ¸ = 45° (c) and ¸ = 70° (d)

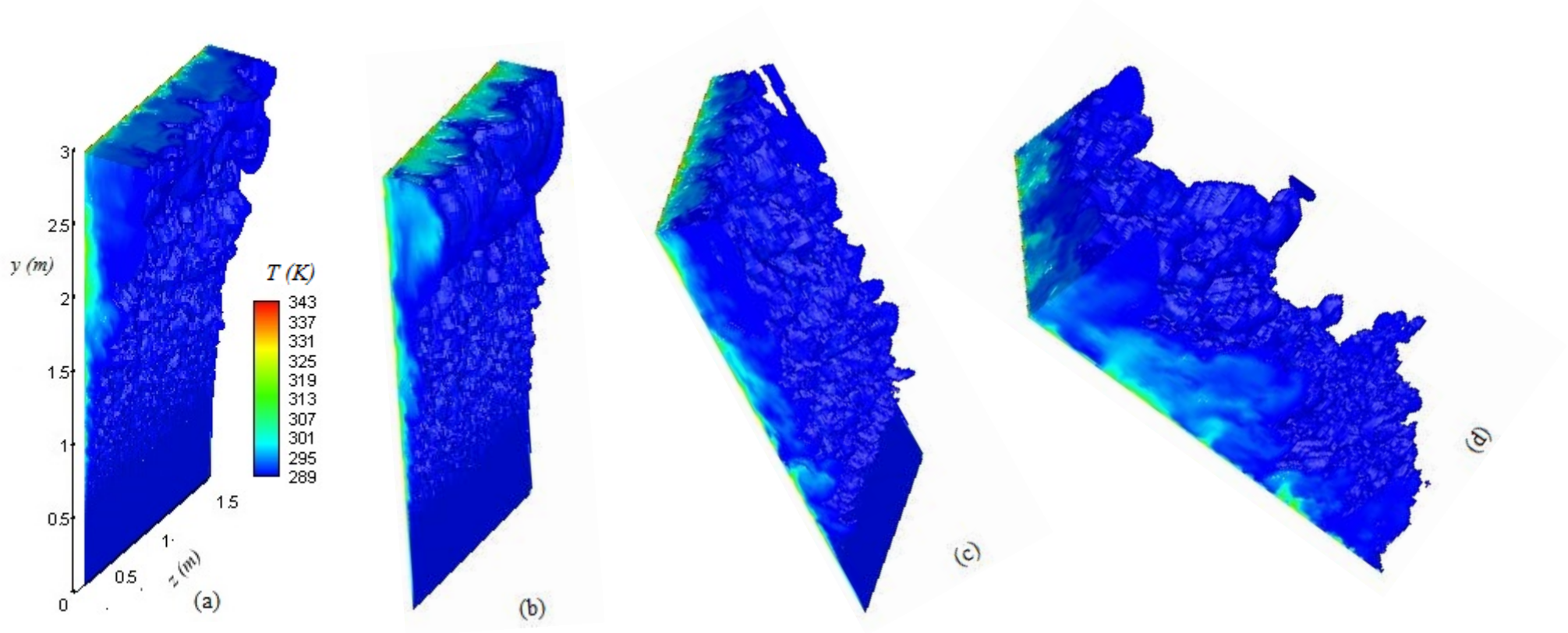

Fig. 6. Temprature iso-surface contour plots at ¸ = 0° (a), ¸ = 20° (b), ¸ = 45° (c) and ¸ = 70° (d)

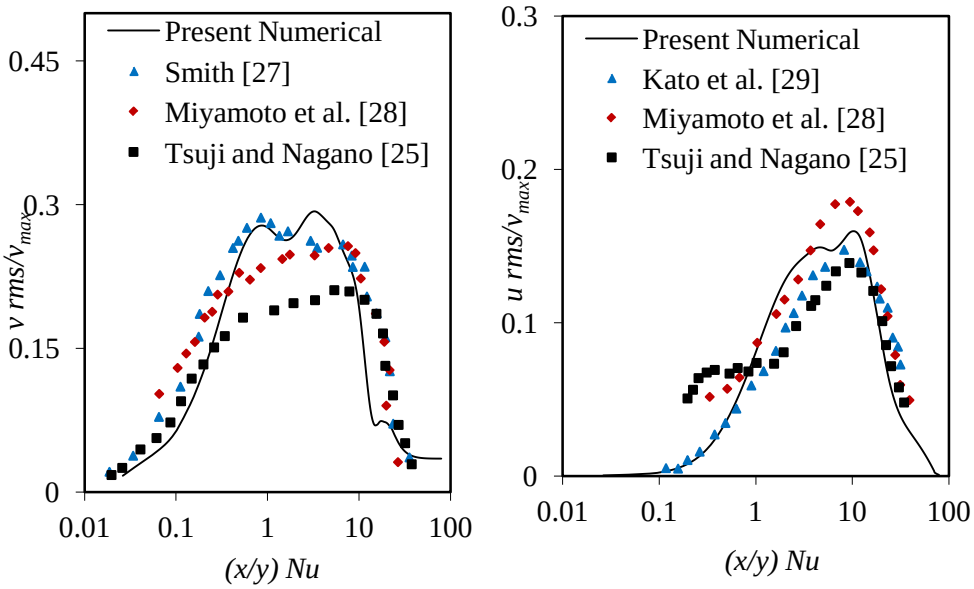

Fig. 7. Comparison of the *rms* of the turbulent velocity fluctuations

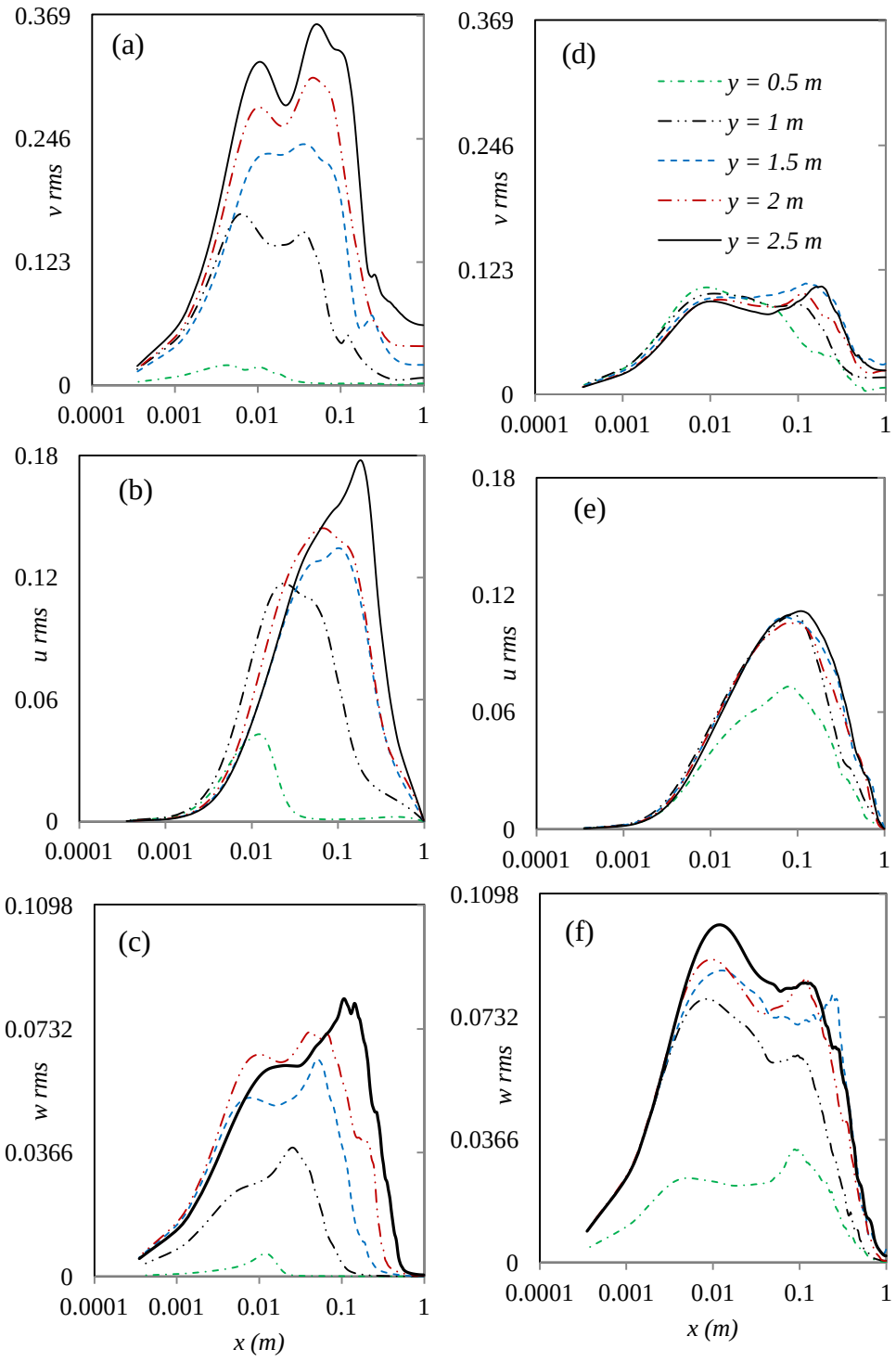

Fig. 8. Profiles of the velocity *rms* at ¸ = 0° (a-c) and ¸ = 70° (d-f)

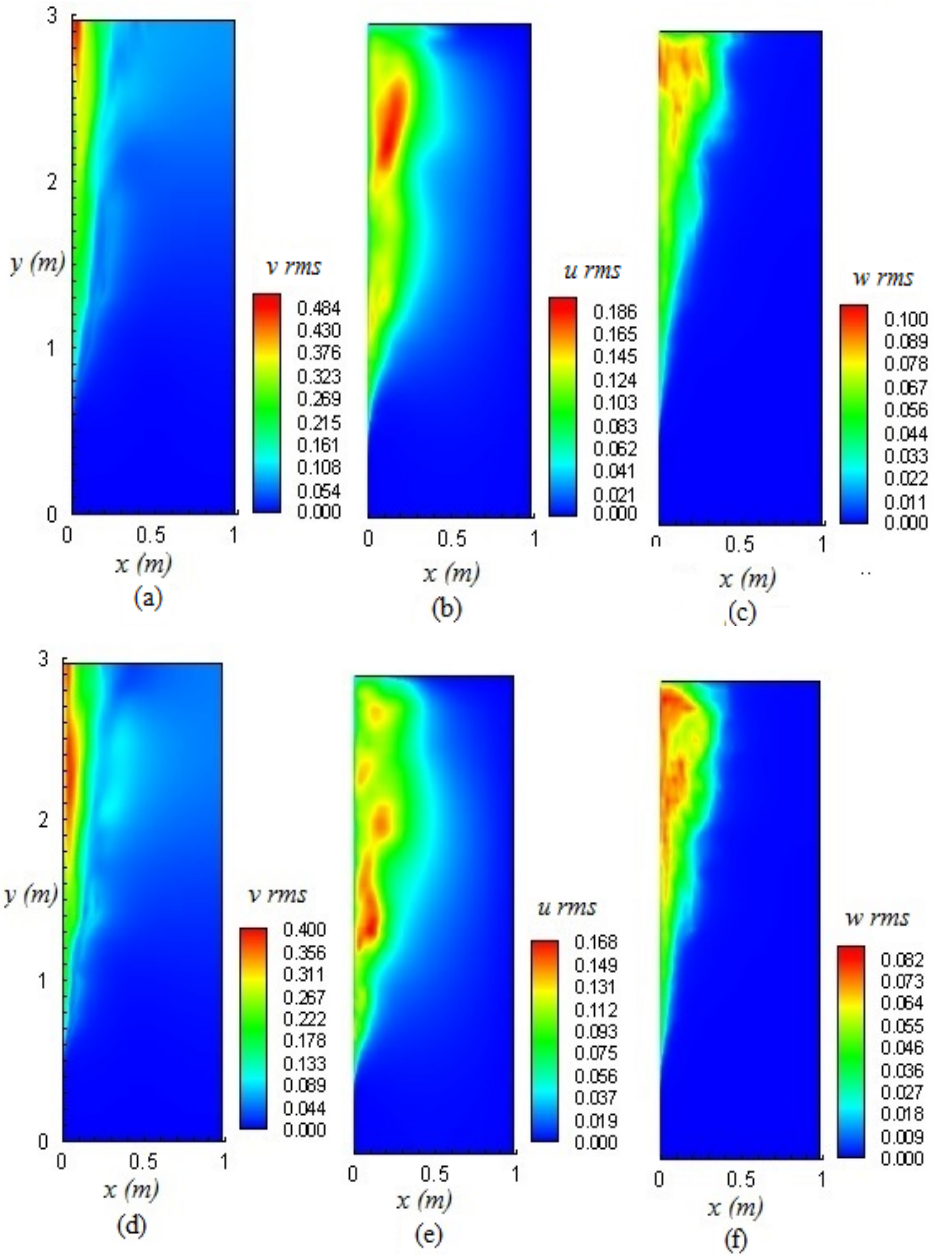

Fig. 9. Contours plot of the velocity *rms* at ¸ = 0° (a-c), ¸ = 20° (d-f), ¸ = 45° (g-i), and ¸ = 70° (j-l).

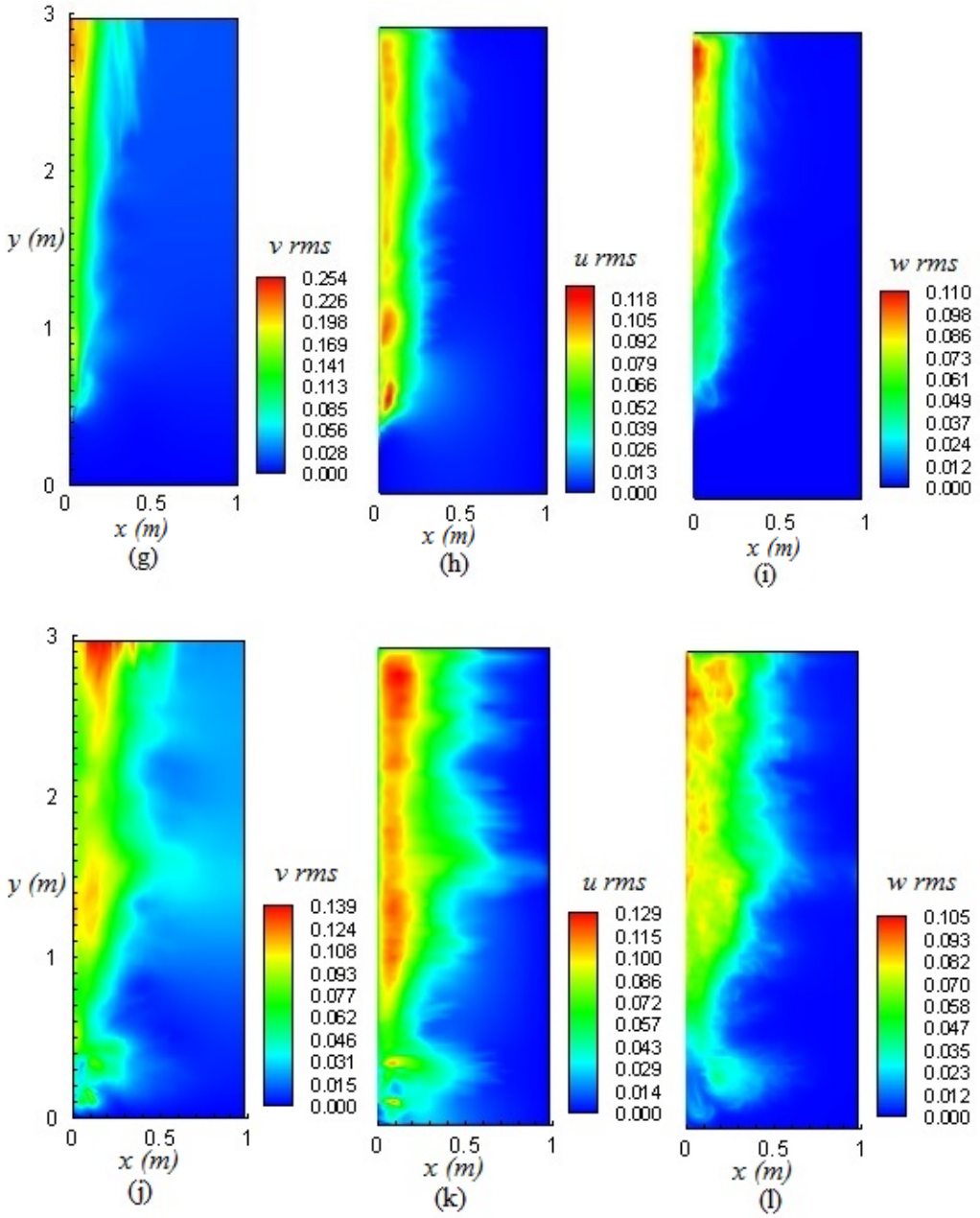

Fig. 9. Caption continued

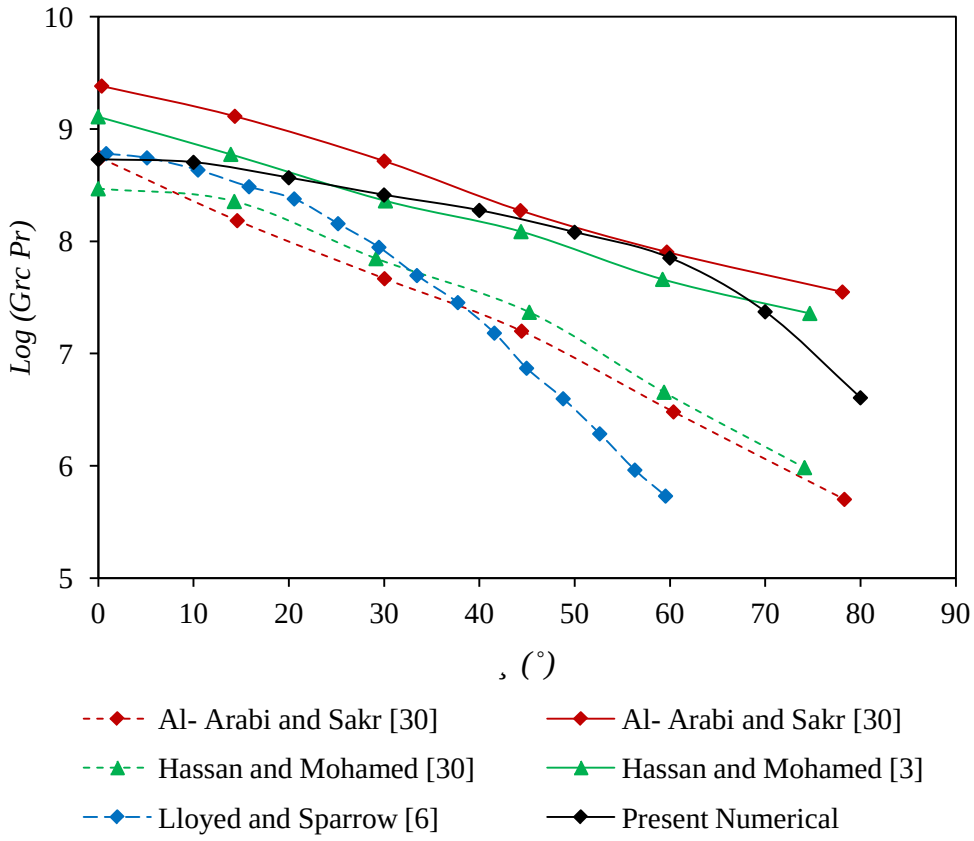

Fig. 10. Critical Grashof number compaired at various angular orienations of the heated plate